World Journal of Advanced Research and Reviews
eISSN: 2581-9615 CODEN (USA): WJARAI
Cross Ref DOI: 10.30574/wjarr
Journal homepage: https://wjarr.com/

(RESEARCH ARTICLE)

High FIBP expression is associated with a ferroptosis-resistant transcriptional phenotype and adverse survival in acute myeloid leukemia: An integrative TCGA-LAML analysis

Meng Tang and Jianxin Guo *

Department of Hematology, The Second Affiliated Hospital of Fujian Medical University, Quanzhou, Fujian, China.

World Journal of Advanced Research and Reviews, 2026, 31(01), 1276–1290

Publication history: Received on 15 June 2026; revised on 20 July 2026; accepted on 23 July 2026

Article DOI: https://doi.org/10.30574/wjarr.2026.31.1.1959

Abstract

Background: FIBP has been linked to adverse acute myeloid leukemia (AML) features, but whether its expression identifies a ferroptosis-related biological state is unknown. We evaluated the association of FIBP with iron handling, lipid-peroxidation defense, immune signatures, and survival while explicitly separating association from causal mechanism.

Methods: The KEGG ferroptosis pathway was compared with the STRING first-shell FIBP network. Legacy TCGA-LAML RNA-sequencing data were analyzed in 173 samples after log2(RSEM+1) transformation. Eleven prespecified genes covering iron homeostasis, antioxidant defense, lipid remodeling, and mitochondrial function were compared across median-defined FIBP groups and correlated with continuous FIBP expression. Marker-derived regulatory T-cell (Treg) and M2-like macrophage scores were examined exploratorily. A ferroptosis sensitivity score was defined as mean Z(TFRC, SLC11A2, ACSL4, LPCAT3) minus mean Z(FTH1, GPX4, AIFM2, DHODH). Overall survival was analyzed in 149 matched patients using Kaplan-Meier estimates, log-rank tests, 3-year restricted mean survival time (RMST), continuous-variable Cox models with proportional-hazards diagnostics, bootstrap-corrected C-index, and time-dependent area under the curve (AUC).

Results: The strict STRING and KEGG sets had no direct gene overlap. Four target genes were higher in FIBP-high AML after transcriptome-wide false-discovery correction: FTH1, GPX4, AIFM2/FSP1, and LPCAT3. FIBP correlated positively with GPX4 (rho=0.619), FTH1 (rho=0.512), LPCAT3 (rho=0.502), and AIFM2 (rho=0.285), and negatively with SLC11A2 (rho=-0.220) and ACSL4 (rho=-0.196). The global FIBP-M2 association was nominal (rho=0.157; P=0.039) but did not remain significant after correction across the two immune scores (q=0.077); the Treg association was not reproduced. Survival differed among low-FIBP, high-FIBP/high-score, and high-FIBP/low-score groups (log-rank P<0.001). Three-year RMST was 729, 492, and 448 days, respectively; the two high-FIBP groups did not differ (RMST difference -44 days; bootstrap 95% CI, -236 to 137). Continuous FIBP remained associated with mortality after adjustment for the score and age (hazard ratio per SD, 1.420; 95% CI, 1.119-1.803; P=0.004), whereas the score was not independently associated (P=0.657). Adding the score did not improve the FIBP-only C-index (0.637 vs 0.636; delta 0.0008, bootstrap 95% CI, -0.0470 to 0.0014).

Conclusions: High FIBP expression is associated with an iron-buffering and antioxidant transcriptional phenotype and adverse survival in AML, but the current data do not demonstrate direct FIBP control of ferroptosis or independent prognostic value of the proposed sensitivity score. GPX4-, FSP1-, and ferritin-centered defenses are testable biological hypotheses rather than established therapeutic indications.

* Corresponding author: Jianxin Guo

Keywords: Acute myeloid leukemia; FIBP; Ferroptosis; Iron metabolism; GPX4; FSP1; Restricted mean survival time; Overall survival

1. Introduction

Acute myeloid leukemia (AML) is a heterogeneous myeloid malignancy characterized by clonal expansion, impaired differentiation, and failure of normal hematopoiesis. Contemporary classification integrates cytogenetic and molecular abnormalities, measurable residual disease, age, fitness, and treatment context, yet substantial outcome variation remains within established risk groups.1 The Cancer Genome Atlas (TCGA) demonstrated that AML contains combinatorial alterations affecting transcription factors, signaling pathways, epigenetic regulators, cohesin, spliceosome components, and tumor suppressors.2 Transcriptomic phenotypes may therefore summarize disease biology not fully represented by individual lesions.

Ferroptosis is an iron-dependent form of regulated cell death caused by uncontrolled phospholipid peroxidation.3 Its execution reflects the balance among redox-active iron, membrane polyunsaturated fatty acids, and antioxidant systems. ACSL4 promotes formation of ferroptosis-sensitive phospholipids,4 whereas GPX4, the CoQ oxidoreductase FSP1, and mitochondrial DHODH establish complementary defense systems.5-7 AML is a plausible setting for ferroptosis-based investigation because leukemic and stem-cell compartments have substantial oxidative and metabolic requirements. GPX4 inhibition suppresses AML growth,8 ferritin-dependent iron homeostasis supports hematopoietic and leukemic stem-cell survival,9 and NCOA4-mediated ferritinophagy is required by quiescent AML stem-cell-enriched populations.10 Additional studies have identified PSTK-, PIEZO1-, FSP1-, and iron-metabolism-dependent resistance programs in AML.11,12,32,33

FIBP encodes FGF1 intracellular binding protein, originally identified as an intracellular partner of mitogenic acidic fibroblast growth factor.13 Later studies linked FIBP to tumor-cell and immune-cell fitness. FIBP was identified as a negative marker of tumor-resilient T cells, and experimental deletion enhanced antitumor cytotoxicity.14 In lung adenocarcinoma, FIBP interacted with STAT3, increased EME1 transcription, and contributed to radioresistance.15 In AML, FIBP was found within a USP5-interacting complex containing C2CD5 and CDK5; however, C2CD5, rather than FIBP, was the functionally validated substrate driving PI3K/AKT/mTOR/HIF-1alpha signaling and glycolysis.16 These observations support biological plausibility but do not establish an AML-specific FIBP mechanism.

Ma and colleagues reported that high FIBP expression in TCGA-LAML was associated with leukocytosis, peripheral-blood blast burden, cytogenetic risk, NPM1 mutation, FAB classification, inferior survival, and immune enrichment.17 Their study establishes precedence and precludes framing FIBP as a newly discovered AML biomarker. The present analysis instead addressed whether FIBP expression is associated with a more specific ferroptosis-related transcriptional phenotype and whether a derived ferroptosis sensitivity score adds prognostic information. We integrated pathway/network resources, TCGA-LAML expression, marker-based immune signatures, contextual clinical results from the prior study, and patient-level survival. The study was explicitly designed as an association-based, hypothesis-generating analysis; no causal mediation or treatment effect was tested.

2. Materials and Methods

2.1. Study design, ethics, and reporting framework

This retrospective integrative study used publicly available, deidentified transcriptomic and clinical data. It was designed as a prognostic-marker and mechanism-generating reanalysis and was reported with reference to the Reporting Recommendations for Tumor Marker Prognostic Studies (REMARK).18 The protocol for the secondary analysis was approved by the Medical Ethics Committee of the Second Affiliated Hospital of Fujian Medical University ([2023]福医附二伦理审字(196)号). No identifiable participant information was accessed, and no additional informed consent was required for analysis of public deidentified data.

2.2. Data sources and analytical cohorts

The human KEGG ferroptosis pathway (hsa04216) provided a 42-gene reference set.20 FIBP-related proteins were defined by the STRING version 12.0 first-shell functional association network, restricted to the 10 highest-ranking partners at a required combined score of at least 0.400.19 STRING edges were interpreted as functional associations rather than necessarily direct physical interactions. Pathway over-representation was calculated against the Enrichr KEGG_2021_Human library by one-sided hypergeometric testing with Benjamini-Hochberg correction.21,22 Because

the enrichment input was itself the KEGG ferroptosis set, enrichment findings were treated as descriptive rather than independent confirmation.

Legacy TCGA-LAML RNA expression data were obtained from the cBioPortal DataHub and contained 173 samples with RSEM abundance values.23,24 Patient-level overall survival and age were obtained from the TCGA-LAML Firehose clinical annotation and matched by the first 12 characters of the TCGA barcode. Overall survival was available for 149 expression-matched patients, including 93 deaths. The expression cohort (n=173) and survival cohort (n=149) were reported separately throughout.

2.3. Expression processing and whole-transcriptome comparison

Expression values were transformed as log2(RSEM+1). When multiple rows mapped to the same canonical gene, the row with greatest across-sample variance was retained. The legacy symbol MRX63 was mapped to ACSL4 using Entrez Gene ID 2182; TfR1, DMT1, and FSP1 were represented by TFRC, SLC11A2, and AIFM2, respectively. Samples were divided at the median FIBP value into 86 low-expression and 87 high-expression samples. Welch two-sample t tests were applied to analyzable genes, with Benjamini-Hochberg false-discovery rate (FDR) control across the transcriptome. A reconstructed differential-expression result required an absolute high-minus-low mean log2 difference greater than 1 and FDR below 0.05. This RSEM-based reconstruction was not an exact replication of the prior HTSeq-count/DESeq2 analysis, which reported 720 differentially expressed genes but did not provide a complete gene-level table in the available materials.17

Table 1 Data sources and analytical cohorts

Analysis layer	Dataset/size	Role in the study
Pathway/network comparison	KEGG ferroptosis: 42 genes; STRING FIBP first shell: top 10	Direct overlap: 0
Expression analysis	173 TCGA-LAML samples	Low FIBP n=86; high FIBP n=87
Reconstructed differential expression	All analyzable genes	263 DEGs: 193 higher, 70 lower
Target-gene analysis	11 prespecified genes	Group FDR and correlation FDR reported separately
Immune reconstruction	173 samples	Treg and M2-like marker scores
Survival analysis	149 matched patients; 93 deaths	Continuous FIBP primary; groups used for visualization/RMST
Published clinical context	151 patients in Ma et al.17	Context only; not pooled with current models

Note: Distinct denominators are reported for expression (n=173) and matched survival (n=149). The Ma et al. cohort is cited as contextual evidence only.

2.4. Prespecified ferroptosis-related gene panel

Eleven genes were prespecified to represent iron handling (TFRC, FTH1, SLC11A2, HAMP), antioxidant or ferroptosis defense (GPX4, AIFM2, DHODH), lipid remodeling (ACSL4, LPCAT3), and mitochondrial function (COX10, OXCT1). High-versus-low group comparisons were taken from the transcriptome-wide analysis. Spearman correlations were calculated between continuous FIBP expression and each target gene; FDR was controlled across the 11 correlations. Correlation coefficients were interpreted as coordinated expression, not evidence of transcriptional regulation.

2.5. Immune-signature reconstruction

Treg and M2-like macrophage states were reconstructed as marker-based expression scores. The Treg score was the mean standardized expression of FOXP3, IL2RA, CTLA4, TIGIT, IKZF2, and TNFRSF18. The M2-like score used CD163, MRC1, MSR1, IL10, CSF1R, and ARG1. Spearman correlations were calculated between each immune score and the 11 target genes, with FDR correction within each 11-gene family. Continuous FIBP was also correlated with the two immune scores, with correction across those two tests. These scores represent transcriptional programs in bulk samples and cannot be interpreted as absolute cell counts or cellular localization.

2.6. Contextual clinical evidence from the published TCGA-LAML study

To avoid combining nonidentical patient-level datasets, clinical associations reported by Ma et al.17 were extracted as contextual evidence and were not pooled with the present expression or survival models. Prespecified contextual features were WBC count, peripheral-blood blast percentage, FAB classification, cytogenetic risk, and NPM1 mutation. Reported odds ratios and P values were reproduced with explicit attribution to the prior study.

2.7. Ferroptosis sensitivity score and risk groups

A higher ferroptosis sensitivity score was intended to indicate greater expression of iron-import/lipid-sensitization genes relative to defense genes. The score was calculated as mean Z(TFRC, SLC11A2, ACSL4, LPCAT3) minus mean Z(FTH1, GPX4, AIFM2, DHODH). FIBP and the score were each divided at their expression-cohort medians. For visualization, patients with survival data were classified as: group A, low FIBP; group B, high FIBP and high score; or group C, high FIBP and low score. The score was exploratory and was derived and evaluated in the same cohort.

2.8. Survival and statistical analysis

Kaplan-Meier curves and an overall log-rank test compared the three visualization groups. Pairwise log-rank P values were adjusted by the Benjamini-Hochberg method. Because Schoenfeld-residual diagnostics indicated nonproportional hazards for the group-B and group-C indicators, group-specific Cox hazard ratios were not used as primary effect estimates. Instead, 3-year restricted mean survival time (RMST; tau=1095 days) and bootstrap 95% confidence intervals were reported for between-group comparisons.27

Continuous FIBP, the continuous ferroptosis score, and age were standardized to 1 SD and analyzed in univariable and multivariable Cox models with Efron handling of ties. Proportional-hazards assumptions were evaluated using correlations between scaled Schoenfeld residuals and log event time.26 Variance inflation factors were calculated to assess collinearity. A spline sensitivity analysis did not identify evidence of nonlinear FIBP association (likelihood-ratio P=0.470); continuous linear FIBP was retained.

Model discrimination was evaluated by Harrell C-index, with 500 bootstrap samples used to estimate optimism and provide sampling intervals.28 Incremental value of the score was assessed by likelihood-ratio testing, change in C-index, and time-dependent cumulative/dynamic AUC using inverse-probability-of-censoring weighting at 1 through 5 years.29 Estimates at late horizons were interpreted cautiously when few patients remained beyond the horizon. An age-adjusted nomogram and quartile-based apparent calibration curves were treated as supplementary exploratory visualizations, not validated clinical tools.

All tests were two-sided. FDR-adjusted $q<0.05$ was used for high-dimensional or prespecified correlation families; nominal $P<0.05$ was used for survival-model coefficients and global tests. Exact P values and 95% confidence intervals were emphasized. Analyses were performed with Python-based scientific and survival-analysis libraries; executable scripts and processed outputs accompany the submission.

3. Results

3.1. Analytical cohorts and absence of direct FIBP-ferroptosis network overlap

The pathway analysis comprised 42 KEGG ferroptosis genes and the 10 highest-ranking STRING first-shell FIBP partners. Their strict intersection was zero (Figure 1; Supplementary Figure S3). Thus, FIBP was not identified as a canonical ferroptosis-pathway member and none of its restricted first-shell partners directly overlapped the KEGG set. The descriptive pathway analysis of the ferroptosis genes yielded 12 FDR-significant KEGG terms, but this reflected biological sharing within a ferroptosis-derived input and was not used as independent evidence of an FIBP-ferroptosis mechanism (Supplementary Figure S4).

The expression cohort contained 173 samples (86 low FIBP and 87 high FIBP). Under the reconstructed threshold, 263 genes differed between groups: 193 were higher and 70 lower in high-FIBP samples (Supplementary Figure S1). These counts differed from the 720 DEGs reported by Ma et al., as expected from the different matrices, sample sets, transformations, and statistical methods.

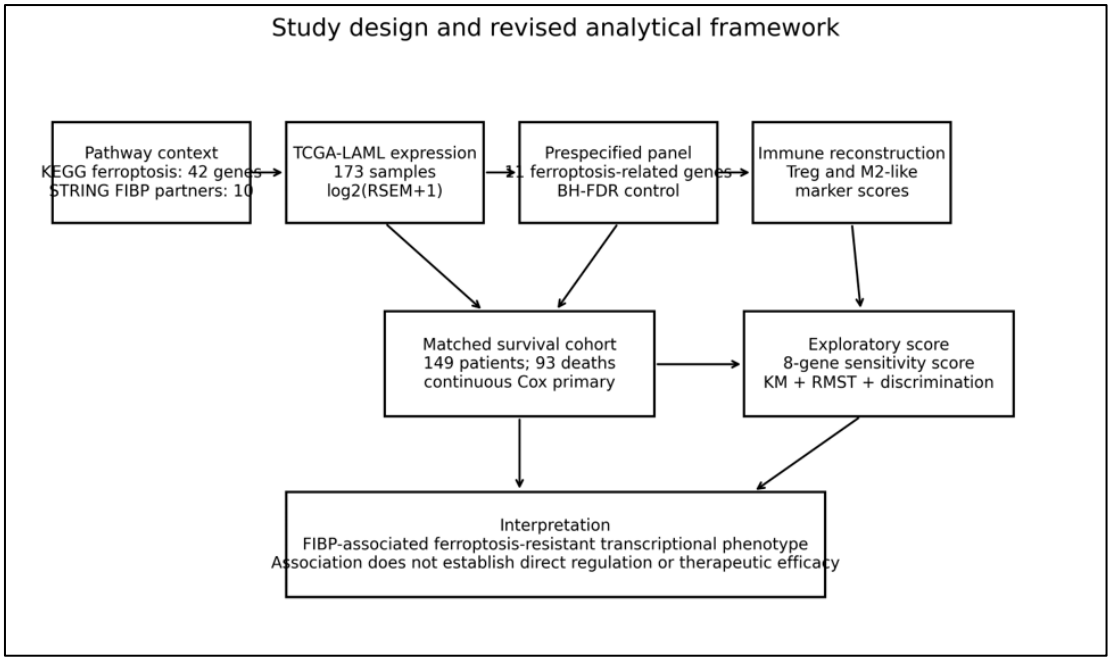

Figure 1 Study workflow and interpretation boundaries. Public pathway/network resources, TCGA-LAML expression, marker-based immune signatures, contextual published clinical results, and matched survival data were integrated. The analysis distinguishes direct network overlap, coordinated transcription, and exploratory clinical associations; no causal mediation was tested

3.2. High FIBP is accompanied by an iron-buffering and antioxidant expression pattern

Among the 11 prespecified genes, FTH1, GPX4, AIFM2/FSP1, and LPCAT3 had transcriptome-wide FDR below 0.05 and were higher in the FIBP-high group (Figure 2A; Table 2). The high-minus-low mean differences were 0.705 for FTH1 (q=8.58x10^-7), 0.604 for GPX4 (q=2.34x10^-10), 0.456 for AIFM2 (q=0.0388), and 0.424 for LPCAT3 (q=2.38x10^-6). None of the 11 genes simultaneously met the more stringent reconstructed requirement of absolute mean difference greater than 1 and q<0.05.

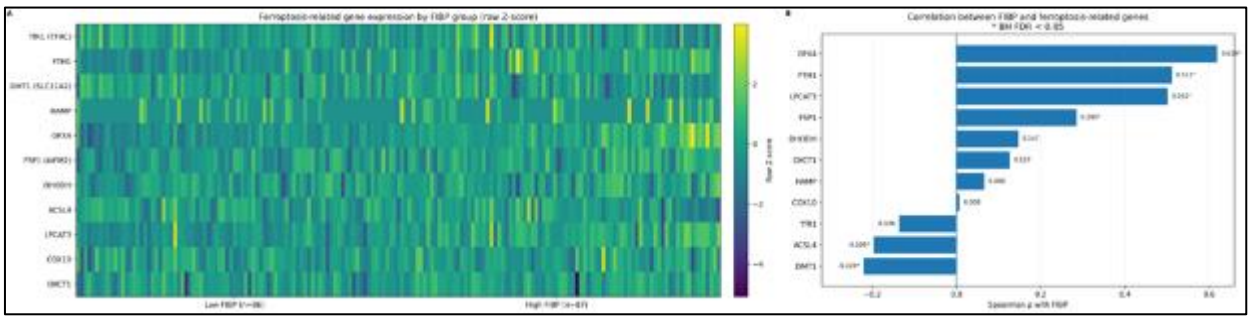

Figure 2 Ferroptosis-related gene expression and correlations with FIBP. (A) Row-standardized expression heatmap for 11 prespecified genes in FIBP-low and FIBP-high samples. (B) Spearman correlations between continuous FIBP and target genes. Asterisks indicate Benjamini-Hochberg FDR below 0.05 across 11 tests

Table 2 Prespecified ferroptosis-related genes: group differences and correlations with FIBP

Gene	Category	High-low Δ	Group q	Spearman rho	Correlation q	Interpretation
TfR1 (TFRC)	Iron homeostasis	-0.080	0.725	-0.136	0.104	Not FDR-significant
FTH1 (FTH1)	Iron homeostasis	0.705	8.58e-07	0.512	3.48e-12	Higher in high FIBP
DMT1 (SLC11A2)	Iron homeostasis	-0.102	0.307	-0.220	0.00814	Lower/inverse association
HAMP (HAMP)	Iron homeostasis	0.127	0.257	0.066	0.423	Not FDR-significant
GPX4 (GPX4)	ROS defense	0.604	2.34e-10	0.619	1.17e-18	Higher in high FIBP
FSP1 (AIFM2)	ROS defense	0.456	0.0388	0.285	0.000386	Higher in high FIBP
DHODH (DHODH)	ROS defense	0.093	0.446	0.147	0.0845	Not FDR-significant
ACSL4 (ACSL4)	Lipid metabolism	-0.107	0.384	-0.196	0.0178	Lower/inverse association
LPCAT3 (LPCAT3)	Lipid metabolism	0.424	2.38e-06	0.502	7.58e-12	Higher in high FIBP
COX10 (COX10)	Mitochondrial function	0.031	0.699	0.008	0.922	Not FDR-significant
OXCT1 (OXCT1)	Mitochondrial function	0.292	0.113	0.127	0.117	Not FDR-significant

Note: Group q values were adjusted across the whole transcriptome; correlation q values were adjusted across the 11 prespecified genes. Δ is the difference in mean log2(RSEM+1). None of the targets met both |Δ|>1 and q<0.05.

Continuous-gene correlations reinforced a coordinated expression pattern (Figure 2B; Supplementary Figure S2). FIBP correlated positively with GPX4 (rho=0.619; q=1.17x10^-18), FTH1 (rho=0.512; q=3.48x10^-12), LPCAT3 (rho=0.502; q=7.58x10^-12), and AIFM2 (rho=0.285; q=3.86x10^-4). Negative correlations were observed for SLC11A2/DMT1 (rho=-0.220; q=0.0081) and ACSL4 (rho=-0.196; q=0.0178). The mixture of higher defense genes and inverse associations with selected iron-import or lipid-sensitization genes was compatible with, but did not prove, a ferroptosis-resistant transcriptional state.

3.3. Immune associations are gene-specific and exploratory

FIBP showed a weak nominal positive correlation with the reconstructed M2-like score (rho=0.157; P=0.0385), but the association did not remain significant after correction across the two immune scores (q=0.0771). The association with the Treg score was negative and nonsignificant (rho=-0.089; P=q=0.247), and therefore did not replicate the positive Treg association reported in the prior ssGSEA-based study.17

Gene-level associations with immune scores were heterogeneous (Figure 3A; Table 3). The M2-like score correlated positively with FTH1 (rho=0.541; q=1.64x10^-13), ACSL4 (rho=0.389; q=4.59x10^-7), LPCAT3 (rho=0.283; q=4.51x10^-4), and SLC11A2 (rho=0.195; q=0.0185), and negatively with DHODH (rho=-0.498; q=1.64x10^-11) and COX10 (rho=-0.212; q=0.0111). The Treg score correlated positively with TFRC (rho=0.298; q=7.47x10^-4) and SLC11A2 (rho=0.239; q=0.00855). These associations did not converge on a single immune-mediated mechanism and were retained as exploratory links for cell-resolved validation.

Table 3 Revised immune-signature results

Comparison	Level	Spearman rho	P value	FDR q
FIBP vs Treg score	Global	-0.089	0.247	0.247
FIBP vs M2-like score	Global	0.157	0.039	0.077
Treg vs TfR1	Gene-level	0.298	6.79e-05	0.000747
M2-like vs FTH1	Gene-level	0.541	1.49e-14	1.64e-13
Treg vs DMT1	Gene-level	0.239	0.00155	0.00855
M2-like vs DMT1	Gene-level	0.195	0.0101	0.0185
M2-like vs DHODH	Gene-level	-0.498	2.99e-12	1.64e-11
M2-like vs ACSL4	Gene-level	0.389	1.25e-07	4.59e-07
M2-like vs LPCAT3	Gene-level	0.283	0.000164	0.000451
M2-like vs COX10	Gene-level	-0.212	0.00505	0.0111

Note: Global FIBP-immune tests were corrected across two scores. Gene-level tests were corrected separately across 11 genes for each immune score. Marker-derived scores do not represent absolute cell abundance.

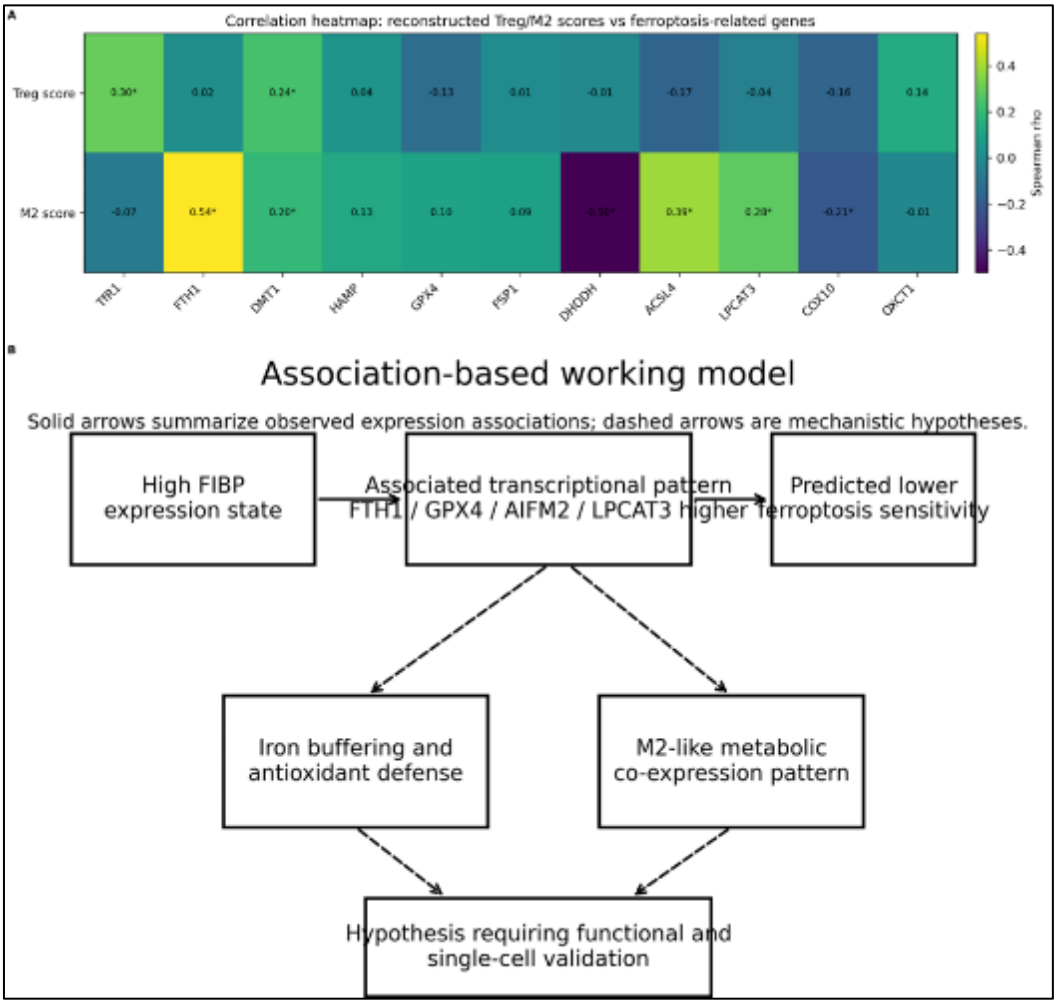

Figure 3 Immune-signature integration and association-based working model. (A) Spearman correlations between marker-derived Treg/M2-like scores and ferroptosis-related genes; asterisks indicate FDR below 0.05 within the 11-gene family. (B) A noncausal working model in which high FIBP marks iron buffering, antioxidant defense, lipid remodeling, immune-context variation, and adverse outcome

3.4. Published clinical findings provide contextual support for an adverse FIBP phenotype

In the prior TCGA-LAML analysis by Ma et al., high FIBP was associated with WBC count above 20x10^9/L (OR, 2.134; P=0.023), peripheral-blood blasts above 70% (OR, 2.722; P=0.003), intermediate/poor versus favorable cytogenetic risk (OR, 5.667; P<0.001), and NPM1 mutation (OR, 2.333; P=0.040).17 FAB distribution also differed overall (P=0.001), and M5 cases were concentrated in the high-FIBP group (14 high vs 1 low). These results were not re-estimated in the present patient-level expression dataset and were used only as contextual support for the hypothesis that FIBP marks a proliferative or monocytic, stress-adapted AML phenotype (Table 4).

Table 4 Contextual clinical associations reported by Ma et al.17

Characteristic	Reported OR	P value	Contextual interpretation
WBC >20 x10^9/L	2.134	0.023	Associated with high FIBP
Peripheral-blood blasts >70%	2.722	0.003	Associated with high FIBP
Intermediate/poor vs favorable cytogenetic risk	5.667	<0.001	Strongest reported association
NPM1 mutation positive vs negative	2.333	0.040	Associated with high FIBP
FAB distribution / M5	Not expressed as one OR	0.001 overall	M5: high FIBP 14 vs low FIBP 1

Note: These are previously published results and were not pooled with the present expression or survival analyses. FAB P value refers to the overall distribution.

3.5. High-FIBP groups have shorter survival, but the score does not separate the high-FIBP strata

Among 149 patients with complete overall-survival data, 80 were in group A, 26 in group B, and 43 in group C; 93 deaths occurred. Median overall survival was 822 days in group A, 365 days in group B, and 273 days in group C. Five-year Kaplan-Meier survival was 30.1%, 21.0%, and 12.2%, respectively. The overall log-rank test was significant (chi-square=14.89; P=5.85x10^-4; Figure 4A). Pairwise FDR-adjusted q values were 0.0126 for A versus B, 0.0010 for A versus C, and 0.544 for B versus C.

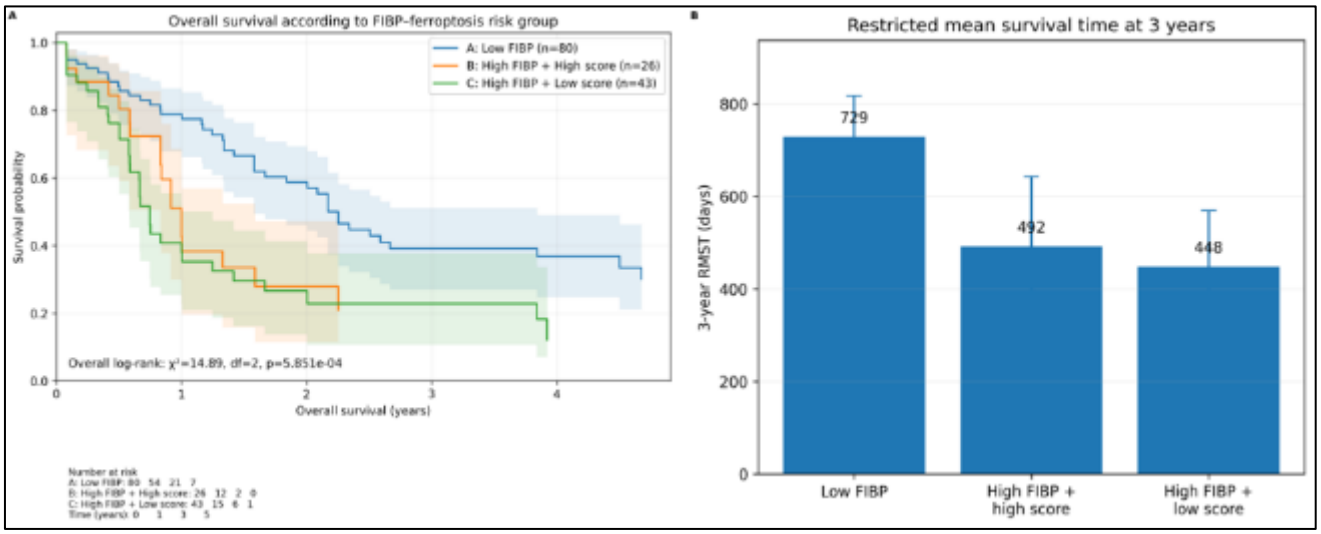

Figure 4 Overall survival by FIBP-ferroptosis visualization group. (A) Kaplan-Meier curves for group A (low FIBP), group B (high FIBP/high score), and group C (high FIBP/low score). The overall log-rank P value is shown. (B) Three-year restricted mean survival time with bootstrap 95% confidence intervals. The B-versus-C RMST difference was not significant

At 3 years, RMST was 729 days (bootstrap 95% CI, 645-817) in group A, 492 days (95% CI, 350-642) in group B, and 448 days (95% CI, 330-569) in group C (Figure 4B). Compared with group A, the RMST deficit was 237 days for group B (95% CI, 60-409 fewer days) and 281 days for group C (95% CI, 132-433 fewer days). The C-versus-B difference was only -44 days (95% CI, -236 to 137). The numerical B-to-C ordering therefore should not be interpreted as validated

risk separation. The three-group Cox indicator model was not retained for primary inference because proportional-hazards diagnostics were significant for both high-FIBP indicators.

3.6. Continuous FIBP, but not the derived score, retains a prognostic association

In univariable Cox analysis, each 1-SD increase in FIBP was associated with higher mortality (HR, 1.402; 95% CI, 1.171-1.678; P=0.00024). The ferroptosis sensitivity score showed a nonsignificant inverse association (HR, 0.822; 95% CI, 0.655-1.031; P=0.091), while age was associated with mortality (HR, 1.762; 95% CI, 1.371-2.264; P<0.001).

When FIBP and the score were entered together, FIBP remained associated with mortality (HR, 1.446; 95% CI, 1.149-1.820; P=0.0017), whereas the score was not (HR, 1.062; 95% CI, 0.810-1.391; P=0.665). After adding age, the HRs were 1.420 for FIBP (95% CI, 1.119-1.803; P=0.0039), 1.063 for the score (95% CI, 0.812-1.392; P=0.657), and 1.708 for age (95% CI, 1.328-2.196; P<0.001) (Figure 5A). No evidence of proportional-hazards violation was detected for these continuous covariates. The FIBP-score Pearson correlation was -0.572, but variance inflation factors were 1.52 for FIBP, 1.49 for the score, and 1.03 for age, providing no evidence of problematic collinearity.

3.7. Adding the score does not improve model discrimination

The apparent C-index was 0.636 for FIBP alone, 0.637 for FIBP plus the ferroptosis score, and 0.678 after adding age (Figure 5B). Optimism-corrected values were 0.634, 0.624, and 0.667, respectively. The apparent C-index increment from adding the score to FIBP was 0.0008, with a bootstrap 95% interval of -0.0470 to 0.0014. The likelihood-ratio test for adding the score was nonsignificant (P=0.666), whereas adding age improved model fit (P<0.001).

Time-dependent AUCs for FIBP alone were 0.723 at 1 year, 0.660 at 3 years, and 0.742 at 5 years. Corresponding values for FIBP plus the score were 0.726, 0.665, and 0.762, and for FIBP plus score plus age were 0.728, 0.726, and 0.799 (Figure 5C). Only eight patients remained event-free beyond the 5-year horizon; late-horizon estimates therefore had substantial uncertainty. The exploratory age-adjusted nomogram and apparent calibration curves were moved to the supplement and were not described as validated prediction instruments (Supplementary Figures S5-S6).

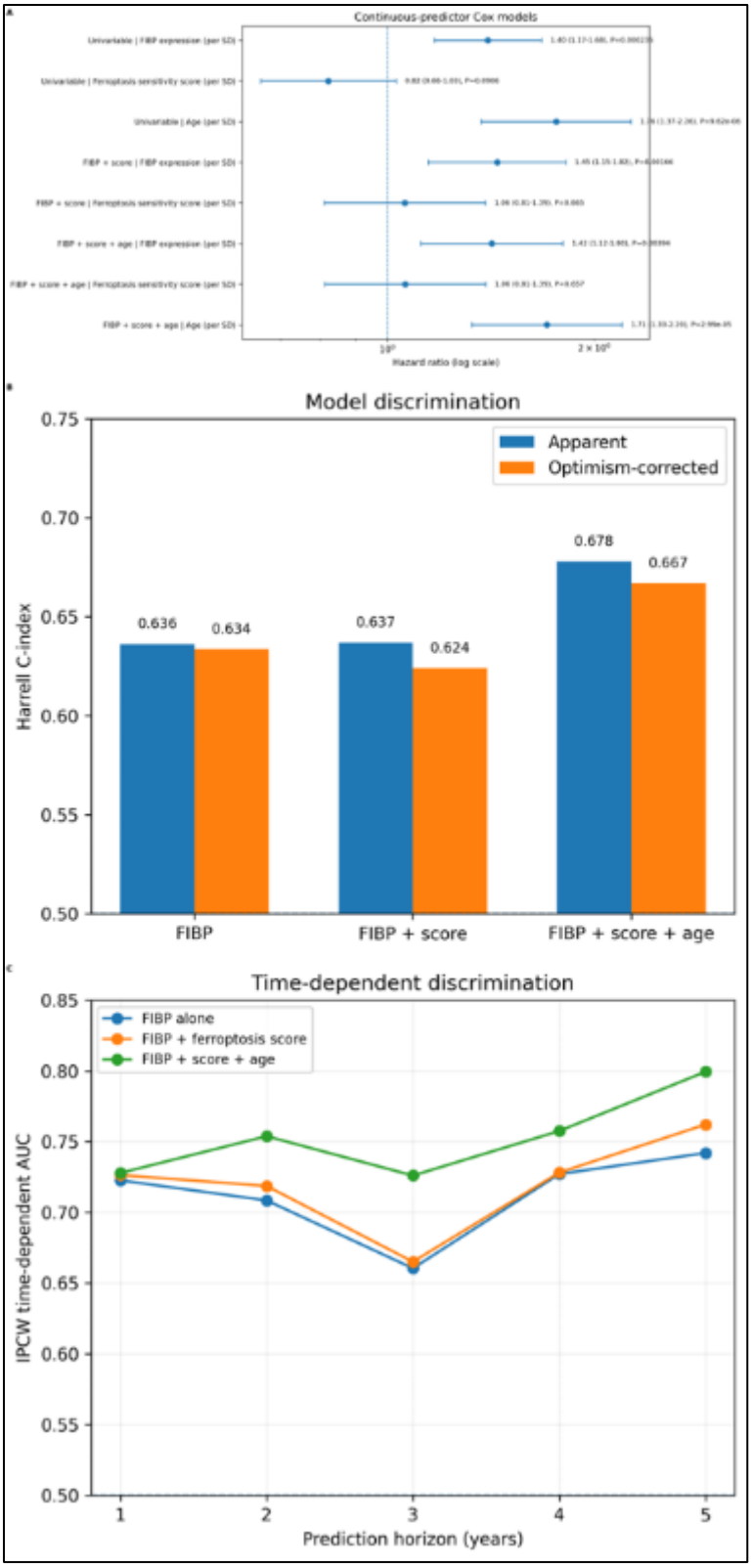

Figure 5 Continuous-variable Cox results and model performance. (A) Univariable and multivariable hazard ratios per 1-SD increase. The continuous models showed no evidence of proportional-hazards violation. (B) Apparent and optimism-corrected Harrell C-indices. (C) IPCW cumulative/dynamic time-dependent AUC at 1-5 years; late estimates are exploratory because few patients remained beyond 5 years

3.8. Association-based working model

The integrated findings support a restrained working model in which high FIBP marks an AML transcriptional state characterized by ferritin-associated iron buffering, GPX4/FSP1 antioxidant defense, and lipid remodeling, accompanied by gene-specific immune associations and adverse outcome (Figure 3B). The model does not establish that FIBP directly regulates these genes, that ferroptosis is functionally suppressed in individual tumors, or that the survival association is mediated by ferroptosis.

4. Discussion

This integrative TCGA-LAML analysis refines the interpretation of FIBP in AML. The strongest finding was not direct pathway membership: the restricted STRING FIBP network and KEGG ferroptosis pathway had no overlapping genes. Rather, high FIBP was accompanied by higher expression of FTH1, GPX4, AIFM2/FSP1, and LPCAT3 and by continuous correlations with several iron- and lipid-peroxidation-related genes. This pattern, together with adverse survival, supports FIBP as a marker of a stress-adapted transcriptional phenotype. It does not establish FIBP-mediated ferroptosis resistance, and the revised title and section headings intentionally use association-based language.

The expression pattern has biological coherence but is not unidimensional. FTH1 can limit the labile iron pool through ferritin storage, while GPX4 and FSP1 suppress lipid peroxidation through distinct biochemical systems.5,6,9 LPCAT3 participates in phospholipid remodeling and may alter the substrate landscape for peroxidation. Conversely, FIBP correlated negatively with SLC11A2 and ACSL4. ACSL4 is a recognized determinant of ferroptosis-sensitive lipid composition,4 and recent work suggests that ACSL4-dependent susceptibility can be particularly relevant in monocytic AML.34 These inverse correlations strengthen the argument that high FIBP marks a composite iron-buffering and antioxidant state, but they also caution against reducing the phenotype to a single “low-ferroptosis” axis. Functional lipidomics, labile-iron measurements, and perturbation studies are required to determine whether this state actually shifts ferroptotic threshold.

The immune analyses were deliberately interpreted more conservatively after multiplicity correction. The global M2-like association was nominal but had q=0.077, and the Treg association was not replicated using the marker-based score. The prior ssGSEA study reported positive FIBP associations with Treg and several innate immune populations,17 but differences in signatures and algorithms can materially alter bulk deconvolution results. In the present data, M2-like associations were gene-specific: FTH1 and ACSL4 were positively related to the M2 score, whereas DHODH and COX10 were negatively related. Bulk expression cannot distinguish malignant monocytic blasts from macrophage programs, nor can it establish that immune cells are protected from ferroptosis. The immune results are therefore best viewed as a roadmap for single-cell RNA sequencing, flow cytometry, spatial profiling, and cell-type-specific iron measurements.

Table 5 Survival and model-performance summary

Analysis	Measure	Estimate	Statistical note
Three-group overall log-rank	-	chi-square 14.89	P=0.000585
3-year RMST, group A	-	729 d (95% CI 645-817)	Low FIBP
3-year RMST, group B	-	492 d (95% CI 350-642)	High FIBP/high score
3-year RMST, group C	-	448 d (95% CI 330-569)	High FIBP/low score
Adjusted FIBP per SD	HR	1.420 (1.119-1.803)	P=0.0039
Adjusted ferroptosis score per SD	HR	1.063 (0.812-1.392)	P=0.657
Adjusted age per SD	HR	1.708 (1.328-2.196)	P=2.99e-05
FIBP-only C-index	Apparent / corrected	0.636 / 0.634	500 bootstrap samples
FIBP + score C-index	Apparent / corrected	0.637 / 0.624	LR test P=0.666
FIBP + score + age C-index	Apparent / corrected	0.678 / 0.667	Exploratory model

Note: Group-specific Cox HRs were removed from primary interpretation because the group-indicator model violated the proportional-hazards assumption. RMST was truncated at 1095 days. Corrected C-index values used 500 bootstrap samples.

Published clinical findings provide an important, but separate, layer of context. Ma et al. associated high FIBP with leukocytosis, high peripheral-blood blast percentage, nonfavorable cytogenetics, NPM1 mutation, and FAB distribution, including enrichment of M5 cases.17 High leukemic burden plausibly increases iron and redox demands, and monocytic differentiation may modify lipid metabolism and ferroptotic susceptibility. However, the present study did not have a harmonized patient-level table containing all of these variables, so the prior odds ratios were not combined with our expression or survival models. This separation avoids pseudo-replication and prevents published associations from being presented as new results.

The survival analysis also changes the interpretation of the proposed ferroptosis score. Low-FIBP patients had longer survival than both high-FIBP groups, but the two high-FIBP groups did not differ by pairwise log-rank testing or 3-year RMST. The high-FIBP/low-score group was numerically worst, but its advantage over the high-FIBP/high-score group was not statistically supported. Moreover, the score was not independently associated with survival after FIBP was included and did not improve C-index or model fit. This result is clinically important because many transcriptomic signatures appear prognostic when dichotomized in their derivation cohort but provide little incremental information beyond a correlated marker.30,31 The score should therefore remain a biological summary for hypothesis generation, not a prognostic classifier.

Continuous FIBP showed the most robust prognostic signal. Its association persisted after adjustment for the exploratory score and age, passed the implemented proportional-hazards diagnostics, and showed no evidence of nonlinearity in sensitivity analysis. Nevertheless, this is limited adjustment. Treatment intensity, transplantation, measurable residual disease, comorbidity, performance status, contemporary ELN risk, and key co-mutations were unavailable or incompletely harmonized. The reported HR therefore reflects an association within the matched public cohort rather than proof that FIBP adds value to a modern clinical-genetic model.

The therapeutic implications should likewise remain conditional. Preclinical AML studies indicate that GPX4, ferritin homeostasis, ferritinophagy, PSTK, PIEZO1-SLC7A11 signaling, FSP1 regulation, and iron mobilization can influence ferroptosis sensitivity.8-12,32,33 These findings provide plausible intervention nodes for testing whether FIBP-high models are preferentially dependent on GPX4/FSP1 or ferritin-associated defenses. A rigorous experimental program would require FIBP knockdown or overexpression in genetically diverse AML models, rescue experiments, lipid ROS and labile-iron assays, pharmacologic and genetic ferroptosis controls, and xenograft studies. Ex vivo samples should be stratified prospectively by FIBP expression before treatment with GPX4/FSP1 or iron-modulating agents. Until such data exist, “targeting iron metabolism” is a research strategy, not a therapeutic recommendation.

This study has several limitations. It is retrospective, single-cohort, and based on a legacy RSEM matrix. The exact 720-gene table from the earlier DESeq2 analysis was unavailable, and our reconstructed differential analysis is methodologically distinct. Immune states were reconstructed from compact marker sets and were not validated against cytometry or single-cell data. The ferroptosis score was constructed and evaluated in the same cohort, creating optimism and limiting transportability. The survival model included only age in addition to molecular variables, and the long-horizon risk sets were small. The three-group indicator model violated the proportional-hazards assumption, necessitating RMST-based interpretation. The nomogram and calibration are apparent internal displays without external validation. Finally, no protein, metabolomic, functional ferroptosis, or perturbation experiments were performed.

Despite these limitations, the study provides a statistically and biologically restrained framework. It distinguishes direct network membership from coordinated expression, separates new analyses from prior clinical evidence, corrects immune findings for multiple testing, diagnoses nonproportional hazards, and formally tests incremental prognostic value. These steps narrow the claim from causal “FIBP-mediated resistance” to an association between FIBP, a ferroptosis-related transcriptional phenotype, and adverse AML outcome.

5. Conclusions

High FIBP expression in TCGA-LAML is associated with higher ferritin/antioxidant-defense gene expression and inferior overall survival. The derived ferroptosis sensitivity score did not independently predict survival or improve discrimination beyond FIBP, and the immune associations were heterogeneous and exploratory. FIBP should therefore be regarded as a candidate marker of a stress-adapted, ferroptosis-related AML state rather than a demonstrated regulator of ferroptosis. Experimental perturbation and external clinical validation are required before iron-directed therapeutic stratification can be proposed.

Abbreviations: AML, acute myeloid leukemia; AUC, area under the curve; FDR, false-discovery rate; FIBP, FGF1 intracellular binding protein; FSP1, ferroptosis suppressor protein 1; HR, hazard ratio; IPCW, inverse probability of censoring weighting; OS, overall survival; RMST, restricted mean survival time; RSEM, RNA-Seq by expectation maximization; TCGA, The Cancer Genome Atlas; Treg, regulatory T cell.

Compliance with ethical standards

Acknowledgments

This study was supported by the 2023 Quanzhou Science and Technology Project (Grant No. 2023NS007).

The authors thank the patients, investigators, and data-generating consortia that contributed to The Cancer Genome Atlas AML project.

Disclosure of conflict of interest

The authors declare no competing interests.

Statement of ethical approval

The protocol for this secondary analysis was reviewed and approved by the Medical Ethics Committee of the Second Affiliated Hospital of Fujian Medical University ([2023]福医附二伦理审字(196)号). The study analyzed publicly available, deidentified data, and no additional informed consent was required.

Statement of informed consent

Informed consent was obtained from all individual participants included in the study."

Data availability

The source RNA-expression data are available from the cBioPortal DataHub TCGA-LAML study, and clinical data are available from the TCGA-LAML Firehose/LinkedOmics portal. Processed tables, figures, statistical diagnostics, and analysis scripts are included in the supplementary submission package and are available from the corresponding author on reasonable request.

Funding

This study was supported by the 2023 Quanzhou Science and Technology Project (Grant No. 2023NS007).

Author contributions

Meng Tang: Conceptualization, methodology, data curation, formal analysis, visualization, and writing - original draft. Jianxin Guo: Conceptualization, validation, supervision, project administration, funding acquisition, and writing - review and editing. Both authors interpreted the results, approved the final manuscript, and agree to be accountable for all aspects of the work.

Use of generative artificial intelligence

A generative artificial intelligence tool was used for language editing, structural organization, and document preparation. It was not used to generate or alter the underlying data or statistical results. The authors reviewed and verified the manuscript, analyses, references, and figures and accept full responsibility for the submitted work.

References

[1] Döhner H, Wei AH, Appelbaum FR, et al. Diagnosis and management of AML in adults: 2022 recommendations from an international expert panel on behalf of the ELN. Blood. 2022;140(12):1345-1377. doi:10.1182/blood.2022016867.

[2] Cancer Genome Atlas Research Network. Genomic and epigenomic landscapes of adult de novo acute myeloid leukemia. N Engl J Med. 2013;368(22):2059-2074. doi:10.1056/NEJMoa1301689.

[3] Dixon SJ, Lemberg KM, Lamprecht MR, et al. Ferroptosis: an iron-dependent form of nonapoptotic cell death. Cell. 2012;149(5):1060-1072. doi:10.1016/j.cell.2012.03.042.

[4] Doll S, Proneth B, Tyurina YY, et al. ACSL4 dictates ferroptosis sensitivity by shaping cellular lipid composition. Nat Chem Biol. 2017;13(1):91-98. doi:10.1038/nchembio.2239.

[5] Bersuker K, Hendricks JM, Li Z, et al. The CoQ oxidoreductase FSP1 acts parallel to GPX4 to inhibit ferroptosis. Nature. 2019;575(7784):688-692. doi:10.1038/s41586-019-1705-2.

[6] Doll S, Freitas FP, Shah R, et al. FSP1 is a glutathione-independent ferroptosis suppressor. Nature. 2019;575(7784):693-698. doi:10.1038/s41586-019-1707-0.

[7] Mao C, Liu X, Zhang Y, et al. DHODH-mediated ferroptosis defence is a targetable vulnerability in cancer. Nature. 2021;593(7860):586-590. doi:10.1038/s41586-021-03539-7.

[8] Akiyama H, Zhao R, Ostermann LB, et al. Mitochondrial regulation of GPX4 inhibition-mediated ferroptosis in acute myeloid leukemia. Leukemia. 2024;38(4):729-740. doi:10.1038/s41375-023-02117-2.

[9] Yi W, Zhang J, Huang Y, et al. Ferritin-mediated mitochondrial iron homeostasis is essential for the survival of hematopoietic stem cells and leukemic stem cells. Leukemia. 2024;38(5):1003-1018. doi:10.1038/s41375-024-02169-y.

[10] Larrue C, Mouche S, Angelino P, et al. Targeting ferritinophagy impairs quiescent cancer stem cells in acute myeloid leukemia in vitro and in vivo models. Sci Transl Med. 2024;16(757):eadk1731. doi:10.1126/scitranslmed.adk1731.

[11] He L, Zhao T, Leong WZ, et al. PSTK inhibition activates cGAS-STING, precipitating ferroptotic cell death in leukemic stem cells. Blood. 2025;145(17):1903-1914. doi:10.1182/blood.2024026040.

[12] Zhang T, Cao Z, Gao K, et al. PIEZO1 is required for acute myeloid leukemia progression and leukemia stem cell maintenance via HIF1A-SLC7A11 axis-mediated ferroptosis defense. Adv Sci (Weinh). 2026. doi:10.1002/advs.75648.

[13] Kolpakova E, Wiedłocha A, Stenmark H, Klingenberg O, Falnes PO, Olsnes S. Cloning of an intracellular protein that binds selectively to mitogenic acidic fibroblast growth factor. Biochem J. 1998;336(Pt 1):213-222. doi:10.1042/bj3360213.

[14] Zhang Y, Vu T, Palmer DC, et al. A T cell resilience model associated with response to immunotherapy in multiple tumor types. Nat Med. 2022;28(7):1421-1431. doi:10.1038/s41591-022-01799-y.

[15] Xu Y, Li J, Zhu K, et al. FIBP interacts with transcription factor STAT3 to induce EME1 expression and drive radioresistance in lung adenocarcinoma. Int J Biol Sci. 2023;19(12):3816-3829. doi:10.7150/ijbs.83134.

[16] Yang Q, Liu JY, Liu SM, Song WJ, Tian YP, Li MY. Deubiquitinase USP5 promotes acute myeloid leukemia through C2CD5 stabilization and PI3K/AKT/mTOR/HIF-1alpha-driven glycolysis. Biochem Pharmacol. 2026;244:117591. doi:10.1016/j.bcp.2025.117591.

[17] Ma M, Xu L, Cui W, Huang Y, Chi G. FIBP is a prognostic biomarker and correlated with clinicopathological characteristics and immune infiltrates in acute myeloid leukemia. Discov Oncol. 2023;14(1):97. doi:10.1007/s12672-023-00723-1.

[18] McShane LM, Altman DG, Sauerbrei W, Taube SE, Gion M, Clark GM. Reporting recommendations for tumor marker prognostic studies (REMARK). J Natl Cancer Inst. 2005;97(16):1180-1184. doi:10.1093/jnci/dji237.

[19] Szklarczyk D, Kirsch R, Koutrouli M, et al. The STRING database in 2023: protein-protein association networks and functional enrichment analyses for any sequenced genome of interest. Nucleic Acids Res. 2023;51(D1):D638-D646. doi:10.1093/nar/gkac1000.

[20] Kanehisa M, Furumichi M, Sato Y, Ishiguro-Watanabe M, Tanabe M. KEGG: integrating viruses and cellular organisms. Nucleic Acids Res. 2021;49(D1):D545-D551. doi:10.1093/nar/gkaa970.

[21] Chen EY, Tan CM, Kou Y, et al. Enrichr: interactive and collaborative HTML5 gene list enrichment analysis tool. BMC Bioinformatics. 2013;14:128. doi:10.1186/1471-2105-14-128.

[22] Benjamini Y, Hochberg Y. Controlling the false discovery rate: a practical and powerful approach to multiple testing. J R Stat Soc Series B. 1995;57(1):289-300.

[23] Cerami E, Gao J, Dogrusoz U, et al. The cBio Cancer Genomics Portal: an open platform for exploring multidimensional cancer genomics data. Cancer Discov. 2012;2(5):401-404. doi:10.1158/2159-8290.CD-12-0095.

[24] Gao J, Aksoy BA, Dogrusoz U, et al. Integrative analysis of complex cancer genomics and clinical profiles using the cBioPortal. Sci Signal. 2013;6(269):pl1. doi:10.1126/scisignal.2004088.

[25] Liu J, Lichtenberg T, Hoadley KA, et al. An integrated TCGA pan-cancer clinical data resource to drive high-quality survival outcome analytics. Cell. 2018;173(2):400-416.e11. doi:10.1016/j.cell.2018.02.052.

[26] Grambsch PM, Therneau TM. Proportional hazards tests and diagnostics based on weighted residuals. Biometrika. 1994;81(3):515-526. doi:10.1093/biomet/81.3.515.

[27] Royston P, Parmar MKB. Restricted mean survival time: an alternative to the hazard ratio for the design and analysis of randomized trials with a time-to-event outcome. BMC Med Res Methodol. 2013;13:152. doi:10.1186/1471-2288-13-152.

[28] Harrell FE Jr, Lee KL, Mark DB. Multivariable prognostic models: issues in developing models, evaluating assumptions and adequacy, and measuring and reducing errors. Stat Med. 1996;15(4):361-387. doi:10.1002/(SICI)1097-0258(19960229)15:4<361::AID-SIM168>3.0.CO;2-4.

[29] Heagerty PJ, Lumley T, Pepe MS. Time-dependent ROC curves for censored survival data and a diagnostic marker. Biometrics. 2000;56(2):337-344. doi:10.1111/j.0006-341X.2000.00337.x.

[30] Cui Z, Fu Y, Yang Z, et al. Comprehensive analysis of a ferroptosis pattern and associated prognostic signature in acute myeloid leukemia. Front Pharmacol. 2022;13:866325. doi:10.3389/fphar.2022.866325.

[31] Tang X, Wang Y, Zhu Y, Guo Y, Liu B. Basic mechanisms and novel potential therapeutic targets for ferroptosis in acute myeloid leukemia. Ann Hematol. 2023;102(8):1985-1999. doi:10.1007/s00277-023-05293-4.

[32] Bian R, Shang Y, Xu N, et al. HDAC inhibitor enhances ferroptosis susceptibility of AML cells by stimulating iron metabolism. Cell Signal. 2025;127:111583. doi:10.1016/j.cellsig.2024.111583.

[33] Ye W, Zhao Y, Zhou Y, et al. NSUN2-mediated cytosine-5 methylation of FSP1 protects acute myeloid leukemia cells from ferroptosis. Mol Cancer. 2025;24(1):201. doi:10.1186/s12943-025-02394-8.

[34] De Marchi F, Gottardi M. ACSL4-driven ferroptosis susceptibility as a targetable vulnerability in monocytic acute myeloid leukemia. Front Oncol. 2026;16:1837940. doi:10.3389/fonc.2026.1837940.